IOPscience iopscience.iop.org

Home Search Collections Journals About Contact us My IOPscience

ZnO nanotube-based dye-sensitized solar cell and its application in self-powered devices

This article has been downloaded from IOPscience. Please scroll down to see the full text article.

2010 Nanotechnology 21 405203

(http://iopscience.iop.org/0957-4484/21/40/405203)

View the table of contents for this issue, or go to the journal homepage for more

Download details:
IP Address: 74.190.213.109
The article was downloaded on 11/09/2010 at 03:11

Please note that terms and conditions apply.

Nanotechnology **21** (2010) 405203 (7pp) doi:10.1088/0957-4484/21/40/405203

ZnO nanotube-based dye-sensitized solar cell and its application in self-powered devices

Jingbin Han[1,2], Fengru Fan[1], Chen Xu[1], Shisheng Lin[1], Min Wei[2,3], Xue Duan[2] and Zhong Lin Wang[1,3]

[1] School of Materials Science and Engineering, Georgia Institute of Technology, Atlanta, GA 30332-0245, USA
[2] State Key Laboratory of Chemical Resource Engineering, Beijing University of Chemical Technology, Beijing 100029, People's Republic of China

E-mail: zhong.wang@mse.gatech.edu (ZLW) and weimin@mail.buct.edu.cn

Received 2 June 2010, in final form 22 August 2010
Published 10 September 2010
Online at stacks.iop.org/Nano/21/405203

Abstract
High-density vertically aligned ZnO nanotube arrays were fabricated on FTO substrates by a simple and facile chemical etching process from electrodeposited ZnO nanorods. The nanotube formation was rationalized in terms of selective dissolution of the (001) polar face. The morphology of the nanotubes can be readily controlled by electrodeposition parameters for the nanorod precursor. By employing the 5.1 μm-length nanotubes as the photoanode for a dye-sensitized solar cell (DSSC), a full-sun conversion efficiency of 1.18% was achieved. Furthermore, we show that the DSSC unit can serve as a robust power source to drive a humidity sensor, with a potential for self-powered devices.

(Some figures in this article are in colour only in the electronic version)

1. Introduction

Dye-sensitized solar cells (DSSC) have been studied extensively as a potential alternative to conventional inorganic solid solar cells, by using nanocrystalline TiO_2 sensitized with ruthenium polypyridine complexes or metal-free organic dyes as photoelectrodes [1–3]. Solar cells based on TiO_2 nanoparticles with a size of 10–30 nm have been used as photoanodes with a demonstrated 11% photovoltaic conversion efficiency [4]. In general, slow electron percolation through the interconnected nanoparticles and the charge recombination between injected electrons and electron acceptors (e.g. I_3^- ions) in the electrolyte hinder the DSSC performance [5]. Considerable efforts have been devoted to the development of more efficient photoanode materials including ordered meso-structured materials [6], one-dimensionally structured materials (nanorod, nanowire, nanotube) [7], etc. Highly ordered TiO_2 nanotube arrays are particularly attractive, which have demonstrated enhanced power conversion efficiency [8–10].

ZnO is another promising but less explored wide bandgap semiconductor oxide used for DSSC. It has similar energy levels to TiO_2. More importantly, its much higher carrier mobility is more favorable for the collection of photoinduced electrons [11, 12]. DSSC built from ZnO nanoparticles shows the second-highest efficiency after TiO_2 [13–16]. Until recently, single-crystal ZnO nanotube arrays were fabricated on transparent conductive substrates by a two-step electrochemical deposition/chemical etching approach [17, 18]. The electrochemical deposition endows low temperature growth, precise control of the morphology and, more importantly, good electrical contact between nanotube arrays and conductive substrates.

Recently, self-powered systems have attracted more and more attention, for such systems could harvest energy from ambient sources and drive electrical devices without external power [19]. Our group has recently demonstrated the harvesting of mechanical energy from ambient sources using piezoelectric ZnO nanowires, which can be applied to power pH and UV sensors without the need for batteries [20]. In the present study, aligned ZnO nanotube arrays were fabricated

[3] Authors to whom any correspondence should be addressed.

 © 2010 IOP Publishing Ltd Printed in the UK & the USA

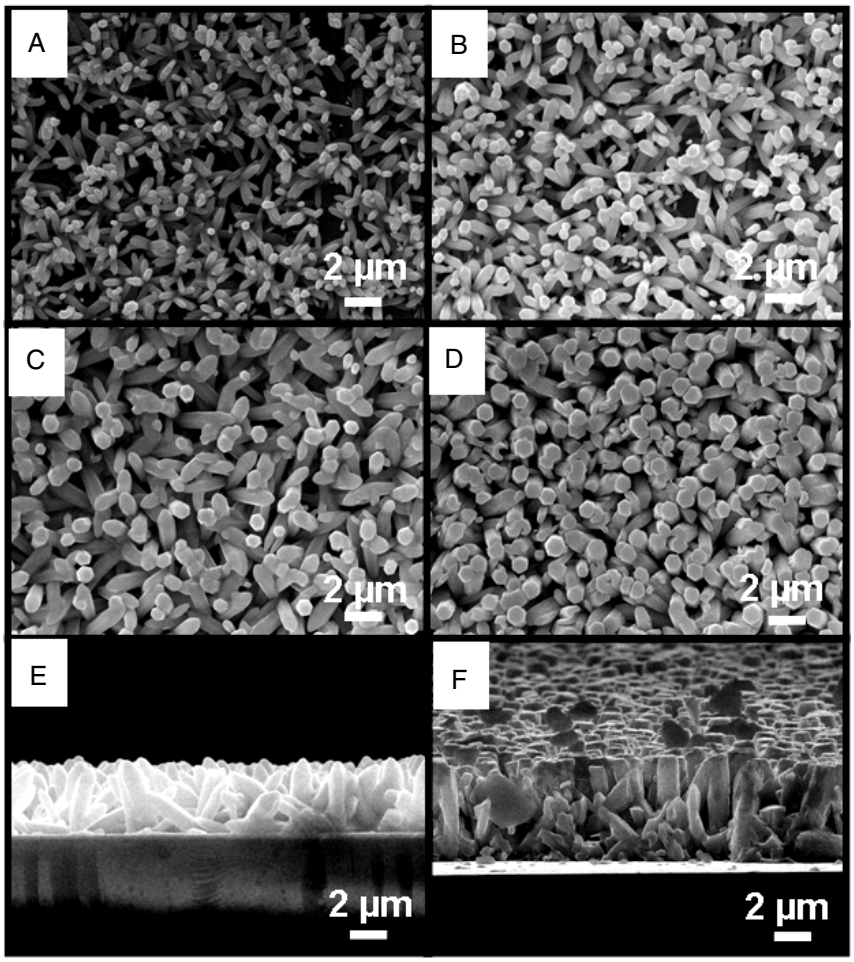

Figure 1. Top-view SEM images of ZnO nanorod arrays obtained by passing different charge densities: (A) 1 C cm^{-2}, (B) 2.5 C cm^{-2}, (C) 5 C cm^{-2} and (D) 10 C cm^{-2}. (E) and (F) Side-view SEM images of (C) and (D), respectively.

by electrochemical deposition of ZnO nanorods followed by chemical etching of the center part of the nanorods. The morphology of the nanotubes can be readily controlled by electrodeposition parameters. By employing the 5.1 μm length nanotubes as photoanodes for DSSC, an overall light-to-electricity conversion efficiency of 1.18% was achieved. In addition, the DSSC can serve as a power source to drive a humidity sensor in a self-powered system. Therefore, this work provides a novel strategy of using solar cells for powering nanodevices.

2. Experimental section

2.1. Synthesis of ZnO nanotubes array on FTO glass

The electrodeposition of a ZnO nanorod array was performed in a three-electrode electrochemical cell with the fluorine-doped SnO_2 transparent conducting oxide (FTO) substrate as the working electrode, a Pt wire as the counter electrode and a saturated calomel electrode (SCE) as the reference electrode. For the working electrode, an area of 2 cm^2 was masked off prior to the deposition. The electrolyte was an aqueous solution of 5 mM $Zn(CH_3COO)_2$ and 3.4 M KCl at pH7. O_2 was continuously bubbled onto the working electrode (FTO-coated glass) surface before and during the whole process. After 10 s of high applied potential at a value of -1.3 V versus SCE in the initial process, the potential applied to the working electrode was stabilized at -1.0 V versus SCE. All the experiments described here were performed at 85 °C, using a VersaSTAT 3 potentiostat. The charge density passing the working electrode ranges from 1 to 10 C cm^{-2}. After the electrodeposition of the ZnO nanorod array, the sample was then immersed in an alkaline solution of 0.125 M KOH at 85 °C for an appropriate period of time and the ZnO nanotube array was subsequently obtained.

2.2. Fabrication of ZnO nanotube DSSC

Prior to the solar cell assembly, the nanotube photoanode was treated with 0.2 M $Zn(OAc)_2$ aqueous solution for 5 min and then annealed at 450 °C for 30 min. Annealed ZnO electrodes were soaked in 0.5 mM of ruthenium (II) dye (known as N719, Dyesol) in a t-butanol/acetonitrile (1:1, v/v) solution for 1 h. The electrodes were washed with acetonitrile, dried and immediately used for assembling the solar cell. To establish the dye loading of the sensitized ZnO nanotube anode, samples sensitized with N719 were placed into a 10 mM solution of

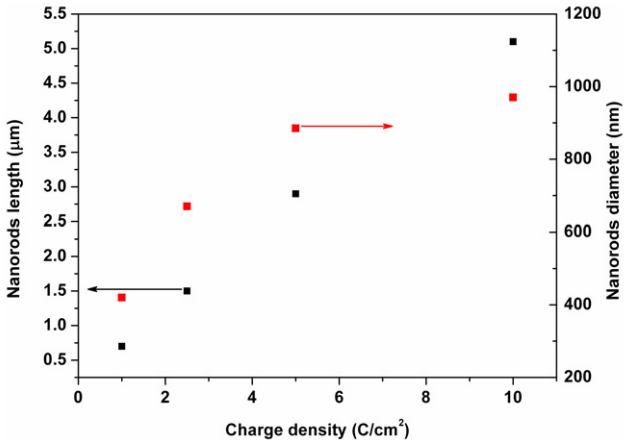

Figure 2. Mean length and diameter of ZnO nanorods as a function of charge density.

KOH (pH13) to desorb the dye. The concentration of desorbed dye determined by UV–vis spectroscopy was used to calculate the amount of dye present in the sensitized nanotube samples. The cell, whose active area was 0.25 cm^2, was fabricated by using the dye-adsorbed ZnO photoanode and a platinized counter electrode. The two electrodes were clipped together and a Himilan film (Solaronix) with 30 μm thickness was used as the spacer. The internal space of the cell was filled with liquid electrolyte by capillary action. The electrolyte was composed of 0.5 M lithium iodide (LiI), 0.05 M iodide (I_2) and 0.5 M 4-*tert*-butylpyridine in 3-methoxypropionitrile. The DSSC was then heated to 120 °C to soften the spacer and seal the edges to prevent the leakage of the electrolyte.

2.3. Preparation of ZnO nanowire humidity sensor

The ZnO nanowires used as a humidity sensor were synthesized in a horizontal furnace with a quartz tube at a pressure around 2200 Pa for 20 min [21], with a length of several tens of micrometers, and widths in the range 100–200 nm. The source material was simply ZnO powder. The sensor was fabricated by laying a ZnO nanowire across the pre-patterned Pt electrodes. The two ends of the nanowire were fixed by conductive silver paste. Humidity-controlled solutions (50 ml) of 96%, 54% H_2SO_4, saturated $Mg(NO_3)_2$, saturated NaCl and saturated KCl were placed in sealed glass chambers of 250 ml, which respectively provide different constant relative humidity (RH) at 25 °C: about 5%, 30%, 54%, 75% and 85% after 24 h.

2.4. Self-powered device

The self-powered device in this study includes the DSSC unit and a humidity sensor, between which aluminum wire was used to form a circuit. The humidity response of the sensor was measured through monitoring the voltage drop across the nanowire as a function of RH. The voltage drop was recorded after the humidity sensor was placed in the chamber with different RH for 1 h. During the measurement, only the sensor part was enclosed in the moisture chamber. At the same time the DSSC unit was exposed to a continuous illumination by a solar simulator.

2.5. Instruments and measurements

The electrochemical deposition of ZnO nanorods was performed on a VersaSTAT 3 potentiostat system. Morphological studies of grown ZnO nanostructures have been performed with a JEOL 2010 TEM operating at 200 kV and a LEO 1550 scanning electron microscope (SEM). X-ray diffraction (XRD) (PANalytical X'Pert PRO Alpha-1) was used to examine the crystal structure of the nanorods. Photovoltaic measurements were recorded employing a solar simulator (300 W Model 91160, Newport) with an AM 1.5 spectrum distribution. The power of the light was calibrated against an NREL reference cell to accurately simulate full-sun intensity (100 mW cm^{-2}). The incident photon-to-electron conversion efficiency (IPCE) measurement was carried out using a 300 W Xe lamp light source coupled to a monochromator (Oriel). A reference Si photodiode calibrated for spectral response was used for the monochromatic power-density calibration. UV–visible absorption spectra were performed on a DU 640 spectrophotometer. Electrochemical impedance spectra (EIS) of fully assembled DSSC were measured in the dark at −0.67 V applied forward bias using a computer-controlled potentiostat (VersaSTAT 3). The spectra were scanned in a frequency range of 0.01 Hz–100 kHz at room temperature with an alternating voltage amplitude set at 10 mV.

3. Results and discussion

Figure 1 shows the highly oriented ZnO nanorod arrays prepared on an FTO-coated glass substrate by passing different charge densities. An increase in the density of the nanorods in the array as a function of the charge density can be observed from the top-view SEM images (figures 1(A)–(D)). The average length of the nanorods was estimated from side-view SEM images, which were representatively shown in figures 1(E) and (F). A considerable increase in nanorod length with the increase of passing charge density was also observed. The mean values (estimated from numerous samples) of the nanorod dimensions corresponding to different charge densities are summarized in figure 2. The ZnO nanorods with a mean length of 0.7, 1.5, 2.9 and 5.1 μm were obtained with a charge density of 1, 2.5, 5 and 10 C cm^{-2}, respectively. Moreover, an increase in mean diameter from 400 to 960 nm was also observed.

Further morphological characterization of the ZnO nanorods was performed by TEM. Figure 3(A) displays a typical TEM image of the ZnO nanorods, which clearly indicates the rod-like morphology of the obtained ZnO sample. The accompanying SAED pattern (see the insert in figure 3(B)) shows that the ZnO nanorod was a single crystal with a hexagonal wurtzite structure. Figure 3(B) presents a high revolution TEM image taken from part of the nanorod. The lattice spacing of 0.52 nm between adjacent lattice planes corresponds to the distance between two [0002] crystal planes, indicating [0001] as the preferred growth direction for ZnO nanorods.

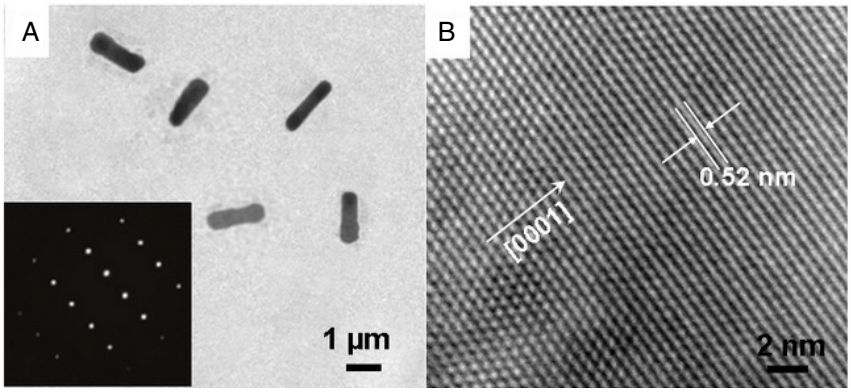

Figure 3. (A) TEM image of the ZnO nanorods. The inset is a selected-area electronic diffraction pattern (SAED) of the nanorods. (B) High revolution TEM image of the ZnO nanorods.

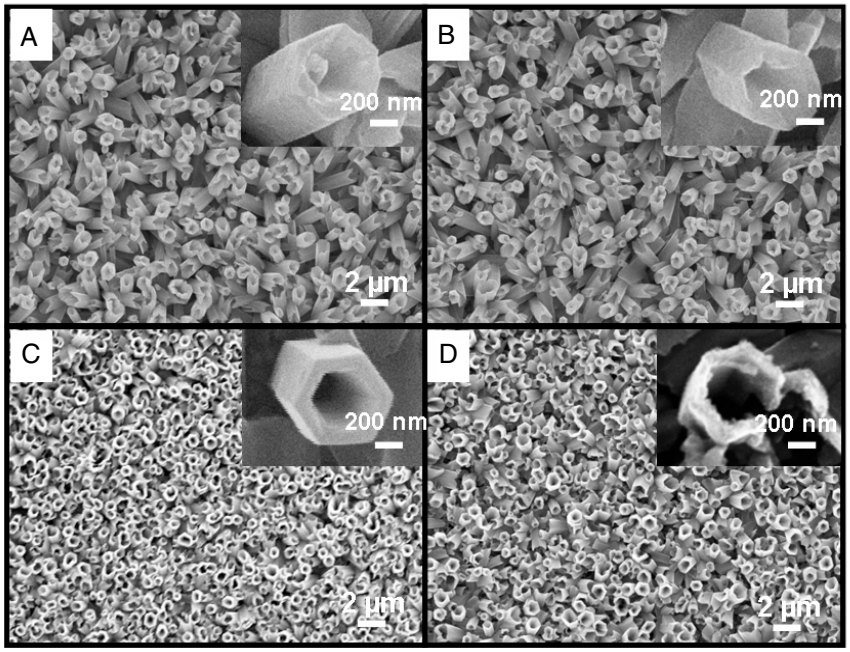

Figure 4. SEM images of the ZnO nanotubes obtained from 2.9 μm length ZnO nanorods via etching in KOH solution for different times: (A) 20 min, (B) 50 min, (C) 80 min and (D) 95 min.

The electrodeposited ZnO nanorods can be transformed into nanotubes after treatment in acidic or alkaline solutions, which is a chemical etching process. The formation of ZnO nanotubes was investigated by etching the 2.9 μm length ZnO nanorods for different times in order to study the dissolution process. Figure 4 shows the morphology of the products at different stages of the etching. It can be seen from figure 4(A) that an etching time of 20 min resulted in a partial dissolution of the core just at the tip. Upon increasing the etching time, the depth of the pit gradually increased, as shown by comparison of samples for 50 and 80 min (figures 4(B) and (C), respectively). As the etching time was longer than 95 min, both the center part and the wall were dissolved (figure 4(D)). It was found that the ZnO nanostructures were fully dissolved and only the FTO-glass substrate remained for times longer than 120 min. The etching time was controlled as 25, 60, 85 and 130 min for 0.7, 1.5, 2.9 and 5.1 μm length nanorods, respectively. Therefore, the hollow ZnO nanotubes can be obtained as long as the etching time was properly controlled, while the length of the nanotubes was almost unchanged after chemical etching. As the dimensions of the electrodeposited ZnO nanorod precursor can be tailored by varying the electrodeposition parameters, the present route offers wide control over the length and the external diameter as well as the depth of the inner pit of the resulting ZnO nanotubes.

Figure 5 displays the x-ray diffraction (XRD) pattern of the ZnO nanotube array on FTO substrates. In this figure, all of the XRD pattern can be indexed as hexagonal wurtzite structures of ZnO. A substantially higher intensity is observed for the [0002] diffraction peak in the XRD pattern of the ZnO sample, indicating that the ZnO nanorods have a preferred orientation along the [0001] direction (perpendicular

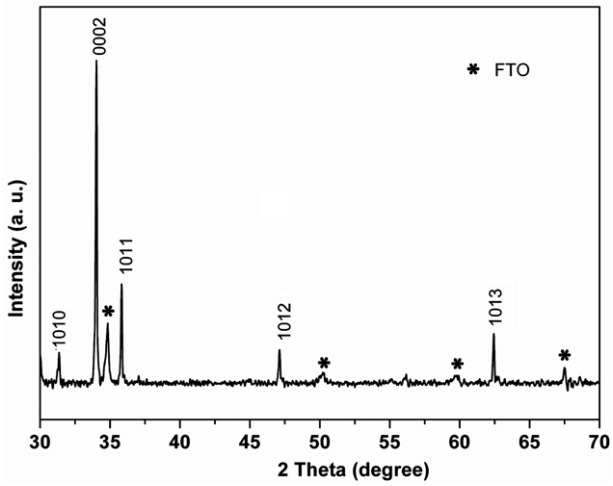

Figure 5. X-ray diffraction pattern of the ZnO nanotube arrays.

to the substrate surface), which has already been confirmed by HRTEM analysis in figure 3(B).

The comparison of surface area available for dye adsorption between nanorods and nanotubes was investigated by measuring the loading of N719 via desorption experiments [10]. The dye loading was calculated to be 1.1, 2.1, 4.9 and 10.7 nmol cm^{-2} for nanorods and 1.9, 4.0, 9.3 and 19.1 nmol cm^{-2} for nanotubes with lengths of 0.7, 1.5, 2.9 and 5.1 μm, respectively. The dye loading is almost twice as high for the nanotubes as that of the nanorods, which is attributed to the additional surface area of nanotubes enclosed inside the hollow structure after the etching process. Taking into account the footprint of 136 $Å^2$ for one single dye molecule adsorbed on the nanotube surface, if one assumes that the experimental dye loading values correspond to monolayer coverage, a surface roughness factor (the real surface area per unit geometric surface area) was obtained to be 156 for a 5.1 μm length nanotube, which is comparable to the reported TiO_2 nanotubes [8].

The current–voltage characteristic curves of DSSC fabricated using ZnO nanotubes with different lengths under simulated AM 1.5 light are shown in figure 6(A). The short-circuit photocurrent densities (J_{sc}) obtained with nanotubes of 0.7, 1.5, 2.9 and 5.1 μm lengths were 0.68, 1.51, 2.50 and 3.24 mA cm^{-2}, respectively. The highest photovoltaic performance of 1.18% (open-circuit voltage $V_{oc} = 0.68$ V and fill factor FF $= 0.58$) was achieved for the sample of 5.1 μm length. This efficiency is attractive, taking into account that the film thickness is only 5.1 μm and no scattering layer is added. The V_{oc} of the DSSC decreases upon increasing the length of the ZnO nanotubes, which is possibly related to the increase in the dark current which scales with the surface area of the ZnO film, in agreement with the previous reports on TiO_2 nanotube-based DSSC [9]. The photon-to-current conversion efficiencies of DSSC using 0.7, 1.5, 2.9 and 5.1 μm length ZnO nanotubes were 0.32%, 0.62%, 0.83% and 1.18%, which were much higher than those of ZnO nanorod DSSCs (i.e. 0.11%, 0.20%, 0.39% and 0.59%). It is worth noting that the conversion efficiency in this work is also higher

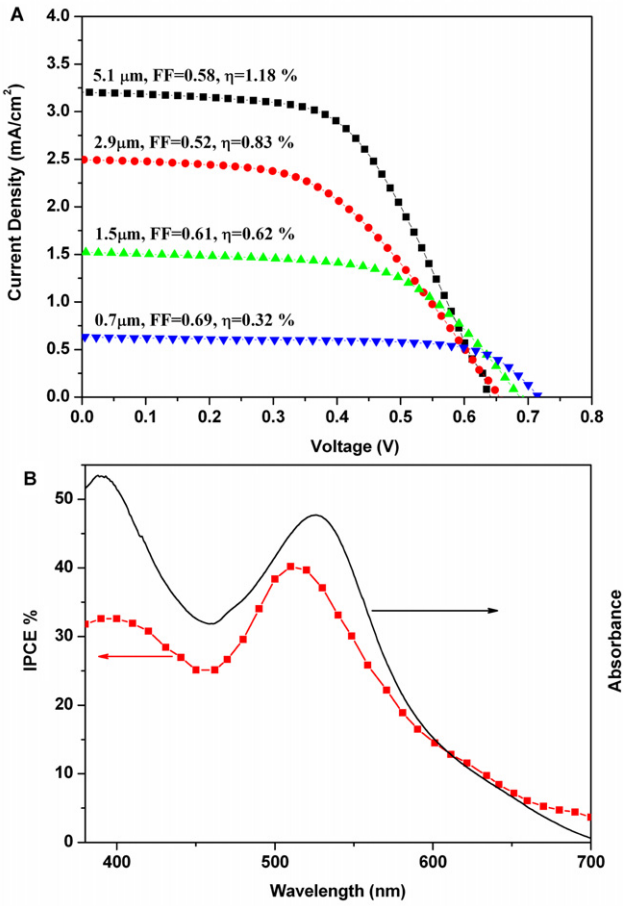

Figure 6. Performance of the DSSC fabricated using ZnO nanotube array film under full-sun illumination: (A) current–voltage characteristic curves of DSSC with various lengths of ZnO nanotubes with $Zn(OAc)_2$ treatment; (B) incident photon-to-current conversion efficiency (IPCE) of a ZnO nanotube-based device (square) and the absorption spectrum of the N719 dye in solution (solid line).

than that of ZnO nanotip array (4.8 μm length)-based DSSC (0.77%) [22]. This is presumably due to the larger available surface area for dye loading of nanotubes than nanorods and nanotips. The photocurrent action spectra (figure 6(B)) display the wavelength distribution of the incident monochromatic photon-to-current conversion efficiency (IPCE). The maximum of IPCE in the visible region is located at ∼520 nm. This is approximately consistent with the expected maximum based on the accompanying absorption spectrum for the N719 dye (with local maxima at 390 and 535 nm), both corresponding to a metal-to-ligand charge transfer transition.

It is well known that the overall conversion efficiency of DSSC can be enhanced by $TiCl_4$ treatment of TiO_2 nanoparticle cells [23–25]. A possible reason is the formation of a blocking TiO_2 layer on the uncovered regions of the FTO to reduce the shunt current, which improves the fill factor. An improved fill factor indicates that this may also be the case for ZnO nanotube-based DSSC. The light-to-electricity conversion efficiency of 0.81% and an FF of 0.51 were achieved by employing ZnO nanotubes (5.1 μm) without $Zn(OAc)_2$ treatment, both lower than that of a

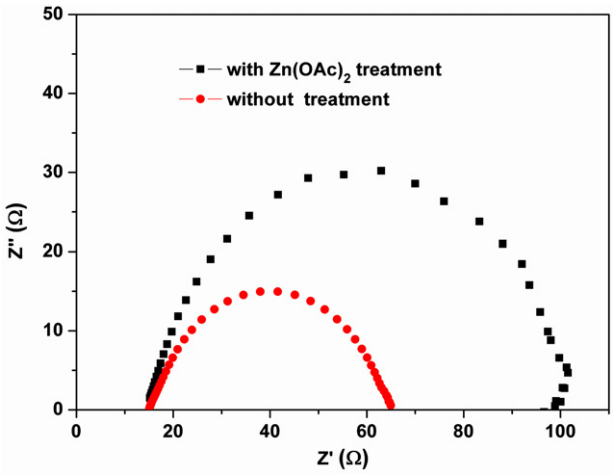

Figure 7. Electrochemical impedance spectra of DSSCs made of ZnO nanotubes with (squares) and without (circles) $Zn(OAc)_2$ aqueous solution treatment, measured at −0.67 V bias in the dark.

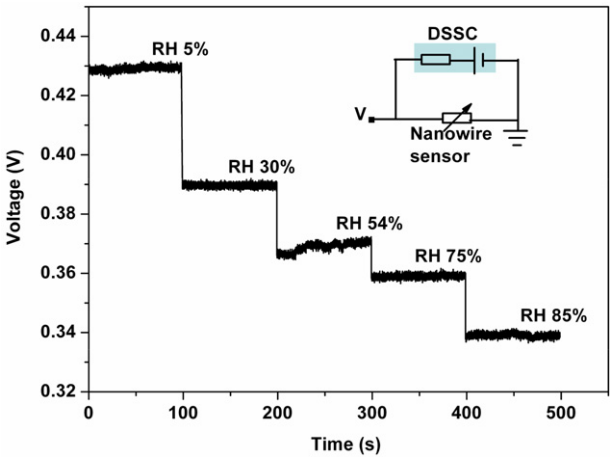

Figure 8. The voltage drop across a humidity sensor as a function of the relative humidity (RH). The sensor was powered by the DSSC. Inset shows the schematic circuit of the 'self-powered' sensor.

treated cell. Furthermore, the electrochemical impedance spectra of the solar cells (figure 7) was measured in the dark to investigate the surface recombination for a solar cell with and without $Zn(OAc)_2$ treatment. The semicircular curve obtained in the intermediate-frequency regime shows the dark reaction impedance caused by electron transport from the ZnO conduction band to the I_3^- ions in the electrolyte [26, 27]. The increased radius of the semicircular curve indicates that the electron recombination resistance increases after $Zn(OAc)_2$ solution treatment, which implies a reduced electron recombination rate at the dye-adsorbed ZnO/electrolyte interface. These results demonstrate the key role of $Zn(OAc)_2$ solution treatment for the enhancement of conversion efficiency.

It has been demonstrated that ZnO nanowires/nanorods could be used as efficient humidity sensors due to the resistance changes when exposed under various relative humidity conditions [28]. Here we demonstrate that the ZnO nanotube solar cell can be used to drive a humidity sensor which is composed of a single ZnO nanowire lying across the Pt electrodes without additional power. The inset of figure 8 shows a schematic circuit of the 'self-powered' sensor. The voltage drop across the sensor (figure 8) shows a decrease as the RH increased, which is related to the decrease of resistance upon increasing RH. This result demonstrates that the DSSC was competent to drive the sensor under illumination of a solar simulator.

4. Conclusions

In summary, a ZnO nanotube array was prepared by chemical etching of electrochemically deposited ZnO nanorods on transparent conductive substrates. The morphology of the ZnO nanotubes can be tuned by varying the deposition conditions of precursor nanorods as well as the etching time. With the treatment of $Zn(OAc)_2$, a full-sun energy conversion efficiency of 1.18% was achieved by employing a 5.1 μm long ZnO nanotube as the photoanode in a DSSC. Further improvement in the cell efficiency should be possible with longer nanotubes. The ZnO nanotube-based DSSC can be used to drive a humidity sensor without external power. Taking into account the wide applications of ZnO nanowires and the variety of nanodevices based on other materials, the device driven by the DSSC unit demonstrated in this study provides a strategy for constructing self-powered systems.

Acknowledgments

This research was supported by BES DOE (DE-FG02-07ER46394), the KAUST Global Research Partnership and NSF (DMS0706436 and CMMI 0403671). JH, FF and SL thank the partial fellowship support by their universities and the China Scholarship Council (CSC) (no. 20073020).

References

[1] O'Regan B and Grätzel M 1991 *Nature* **353** 737
[2] Chen C-Y, Wu S-J, Li J-Y, Wu G, Chen J-G and Ho K-C 2007 *Adv. Mater.* **19** 3888
[3] Freitas J N, Nogueira A F and Paoli M-A D 2009 *J. Mater. Chem.* **19** 5279
[4] Nazeeruddin M K, Angelis F D, Fantacci S, Selloni A, Viscardi G, Liska P, Ito S, Takeru B and Grätzel M 2005 *J. Am. Chem. Soc.* **127** 16835
[5] Katoh R, Furube A, Kasuya M, Fuke N, Koide N and Han L 2007 *J. Mater. Chem.* **17** 3190
[6] Chen D, Huang F, Cheng Y-B and Caruso R A 2009 *Adv. Mater.* **21** 2206
[7] Mor G K, Varghese O K, Paulose M and Grimes C A 2005 *Adv. Funct. Mater.* **15** 1291
[8] Kang T-S, Smith A P, Taylor B E and Durstock M F 2009 *Nano Lett.* **9** 601
[9] Varghese O K, Paulose M and Grimes C A 2009 *Nat. Nanotechnol.* **4** 592
[10] Jennings J R, Ghicov A, Peter L M, Schmuki P and Walker A B 2008 *J. Am. Chem. Soc.* **130** 13364
[11] Zhang Q, Dandeneau C S, Zhou X and Cao G 2009 *Adv. Mater.* **21** 4087

[12] Seow Z L S, Wong A S W, Thavasi V, Jose R, Ramakrishna and Ho G W 2009 *Nanotechnology* **20** 045604
[13] Zhang Q, Chou T P, Russo B, Jenekhe S A and Cao G 2008 *Angew. Chem. Int. Edn* **47** 2402
[14] Rao A R and Dutta V 2008 *Nanotechnology* **19** 445712
[15] Weintraub B, Wei Y and Wang Z L 2009 *Angew. Chem. Int. Edn* **48** 8981
[16] Bacsa R R, Dexpert-Ghys J, Verelst M, Falqui A, Machado B, Bacsa W S, Chen P, Zakeeruddin S M, Gräetzel M and Serp P 2009 *Adv. Funct. Mater.* **19** 875
[17] She G-W, Zhang X-H, Shi W-S, Fan X, Chang J C, Lee C-S, Lee S-T and Liu C-H 2008 *Appl. Phys. Lett.* **92** 053111
[18] Elias J, Tena-Zaera R, Wang G-Y and Lévy-Clément C 2008 *Chem. Mater.* **20** 6633
[19] Wang Z L and Song J H 2006 *Science* **312** 242
[20] Xu S, Qin Y, Xu C, Wei Y, Yang R and Wang Z L 2010 *Nat. Nanotechnol.* **5** 366
[21] Gao Z, Ding Y, Lin S, Hao Y and Wang Z L 2009 *Phys. Status Solidi (RRL)* **3** 260
[22] Chen H, Pasquier A D, Saraf G, Zhong J and Lu Y 2008 *Semicond. Sci. Technol.* **23** 045004
[23] Liu B and Aydil E S 2009 *J. Am. Chem. Soc.* **131** 3985
[24] Ito S *et al* 2005 *Chem. Commun.* 4351
[25] Fuke N *et al* 2009 *Energy Environ. Sci.* **2** 1250
[26] Zhang W, Zhu R, Liu X, Liu B and Ramakrishna S 2009 *Appl. Phys. Lett.* **95** 043304
[27] Wang Q, Moser J E and Grätzel M 2005 *J. Phys. Chem.* B **109** 14945
[28] Zhang Y, Yu K, Jiang D, Zhu Z, Geng H and Luo L 2005 *Appl. Surf. Sci.* **242** 212